

$W^\pm b\bar{b}$ production in POWHEG

Carlo Oleari

*Università di Milano-Bicocca and INFN, Sezione di Milano-Bicocca
Piazza della Scienza 3, 20126 Milan, Italy
E-mail: Carlo.Oleari@mib.infn.it*

Laura Reina

*Department of Physics, Florida State University
Tallahassee, FL 32306-4350, U.S.A.
E-mail: reina@hep.fsu.edu*

ABSTRACT: We present an implementation of the next-to-leading order hadronic production of a W^\pm boson in association with a pair of massive bottom quarks in the framework of POWHEG, a method to consistently interface NLO QCD calculations with shower Monte Carlo generators. The process has been implemented using the POWHEG BOX, an automated computer code that systematically applies the POWHEG method to NLO QCD calculations. Spin correlations in the decay of the W^\pm boson into leptons have been taken into account using standard approximated techniques. We present phenomenological results for $Wb\bar{b} \rightarrow l\nu b\bar{b}$ production, at both the Tevatron and the LHC, obtained by showering the POWHEG results with PYTHIA and HERWIG, and we discuss the outputs of the two different shower Monte Carlo programs.

KEYWORDS: QCD, Monte Carlo, NLO Computations, Resummation, Collider Physics

Contents

| | |
|---|-----------|
| 1. Introduction | 1 |
| 2. Construction of the POWHEG implementation | 3 |
| 2.1 The next-to-leading order cross sections | 3 |
| 2.2 The POWHEG BOX ingredients | 4 |
| 2.3 Validation of the NLO code | 4 |
| 3. Theoretical introduction | 5 |
| 3.1 Generation of the underlying Born configuration | 5 |
| 3.2 Generation of the radiation variables | 5 |
| 3.3 Tuning of the real contribution | 6 |
| 3.4 $Wb\bar{b}$ production | 6 |
| 3.5 W -boson decay | 9 |
| 4. Phenomenology | 12 |
| 4.1 Tevatron results | 14 |
| 4.2 LHC results | 16 |
| 5. Conclusions | 18 |

1. Introduction

The production of a W^\pm boson in association with a pair of massive bottom quarks (b and \bar{b}), contributing to both the $W + 1 b$ -jet and $W + 2 b$ -jets signatures, represents both an interesting Standard Model signal and one of the most important background processes for single-top production and Higgs searches.

The cross sections for W boson production with bottom quarks has been measured at the Tevatron $p\bar{p}$ collider at Fermilab by both the CDF [1] and D0 [2] Collaborations. As more data will be collected and analyzed by the Tevatron Collaborations, we will gain increasing precision in the cross section measurements and we will have a unique opportunity to test and improve the theoretical description of heavy-quark jets at hadron colliders by performing a thorough comparison between the Tevatron experimental data and existing theoretical predictions. Studying the same cross sections in the very different kinematic regimes available at the LHC pp collider will then be of great interest and will represent a crucial test of our understanding of QCD at high-energy colliders.

Moreover, the production of a W boson with one or two b jets represents a crucial irreducible background for both single-top production ($p\bar{p}, pp \rightarrow t\bar{b}, \bar{t}b$) and Higgs-boson

associated production (WH), followed by the decay $H \rightarrow b\bar{b}$. We remind that WH associated production is the most sensitive Higgs-boson production channel at the Tevatron, while it is a difficult, but very important, channel at the LHC, where, in particular kinematic regions (boosted H), can provide essential additional signal for the detection of a low-mass Higgs boson [3, 4, 5].

It is therefore crucial to have the $W + b$ -jets background theoretically under good control. Several steps have already been taken towards this goal. At the parton level, the production of a W boson with up to two jets, one of which is a b jet, has been calculated including next-to-leading-order (NLO) QCD corrections in the variable-flavor scheme [6], while the production of a W boson with two b jets has been computed at NLO in QCD using the fixed-flavor scheme, first in the massless b -quark approximation [7, 8, 9, 10] and more recently including full b -quark mass effects [11, 12, 13, 14]. The two calculations have been combined in ref. [15] to provide the most accurate theoretical predictions for $W + 1 b$ -jet production. The comparison with the experimental measurement of the total cross section for W plus at least one b jet shows a clear discrepancy [1, 16, 17] which should be further investigated, given the importance of this background, in particular for Higgs boson searches. A few predictions for $W + 2b$ jets at NLO in QCD can be found in ref. [11] for the Tevatron and in ref. [13] for the LHC, and are available to the experimental community for comparison.

The Standard Model prediction for $Wb\bar{b}$ production could be further improved by properly interfacing the parton level NLO calculation with a parton shower (PS) simulation. An event generator of this nature should also be beneficial in understanding other experimental systematics for which parton shower simulations are relied upon, including the transverse momentum and rapidity distributions of b jets and hard non- b jets, as well as the angular separation and invariant-mass distribution of the two b -jet system, often used in experimental analyses to enhance the signal to background ratio.

In recent times, the construction of these NLO+PS event generators has become viable: see, e.g., `MC@NLO` [18] and `POWHEG` [19, 20]. The effectiveness of the `POWHEG` approach has been demonstrated successfully and studied in some detail through its application to a substantial array of hadron collider processes (see, for example, [21, 22, 23, 24, 25, 26, 27, 28, 29, 30, 31, 32, 33, 34, 35]). In this paper we interface the NLO calculation of the cross section for $Wb\bar{b}$ production to a shower Monte Carlo program within the `POWHEG` framework. This is the first time that such calculation has been performed: more specifically, we have implemented this process using the `POWHEG BOX` [36], a general computer code framework for embedding NLO calculations into shower Monte Carlo programs according to the `POWHEG` method. Spin correlations in the decay of the vector boson into leptons have been taken into account using standard approximated techniques [37]. We have checked that we have very good agreement between our approximated result and the NLO calculation for $Wb\bar{b} \rightarrow l\nu b\bar{b}$ production of ref. [14], where spin correlations have been taken into account exactly.

The paper is organized as follows. In section 2 we give a brief description of the `POWHEG` implementation of the $Wb\bar{b}$ process and of the needed ingredients. Since we use the `POWHEG BOX` to implement our process, we refer the reader to the `POWHEG BOX` publication [36], and we report here only those aspects of the implementation that are particularly relevant to

the process in question. In section 3, after briefly recalling how POWHEG generates an event and how the POWHEG BOX deals with the presence of Born-zero configurations, we illustrate how we have implemented the decay of the W boson. In section 4 we present and discuss a few results for the Tevatron and the LHC, where the POWHEG-generated events are showered by PYTHIA and HERWIG. Finally, in section 5, we summarize our results and give our final remarks.

2. Construction of the POWHEG implementation

2.1 The next-to-leading order cross sections

The NLO QCD corrections to $q\bar{q}' \rightarrow Wb\bar{b}$ production consist of both one-loop virtual corrections to the tree level processes depicted in fig. 1 and one-parton real radiation from both the initial- and final-state quarks, i.e. $q\bar{q}' \rightarrow Wb\bar{b} + g$. At the same order, the $qg(g\bar{q}') \rightarrow Wb\bar{b} + q'(\bar{q})$ processes also need to be included. The $\mathcal{O}(\alpha_s^2)$ virtual corrections

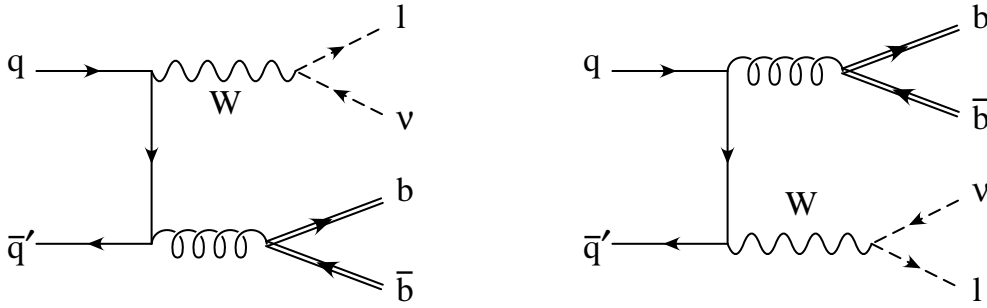


Figure 1: The tree-level Feynman diagrams for $q\bar{q}' \rightarrow Wb\bar{b}$.

consist of self-energy, vertex, box and pentagon diagrams. Dimensional regularization is used to regularize both UV and IR singularities. The UV singularities are cancelled by introducing a suitable series of counterterms. We renormalize the wave functions of the external massive quarks in the on-shell scheme, and the strong coupling constant α_s in the mixed scheme of ref. [38], in which the heavy-flavour top loop is subtracted at zero momentum, while all the other flavours are subtracted in the $\overline{\text{MS}}$ scheme. Self-energy, vertex, box and pentagon diagrams contain IR divergences that combine and cancel against the soft and collinear divergences in the real-emission corrections, when computing infrared-safe quantities with renormalized parton distribution functions (pdf). More details on the calculation of the $\mathcal{O}(\alpha_s^2)$ virtual corrections can be found in refs. [11, 12, 13].

While in refs. [11, 12, 13] the W boson is not decayed and is produced on-shell, the POWHEG BOX implementation of $Wb\bar{b}$ production includes the leptonic decay of the W , in an approximated way, as described in section 3.5. To implement this, the analytic results of refs. [11, 12, 13] have been modified to lift the W on-shell condition and the invariant mass of the W boson has been generated according to a Breit-Wigner distribution function.

2.2 The POWHEG BOX ingredients

We have implemented the NLO QCD cross section for $Wb\bar{b}$ production into the POWHEG BOX environment by providing the following ingredients:

- i. the list of all flavour structures of the Born processes;
- ii. the list of all flavour structures of the real processes;
- iii. the squared Born amplitude \mathcal{B} and the colour correlated ones \mathcal{B}_{ij} ¹;
- iv. the Born phase space;
- v. the squared real matrix elements for all relevant partonic processes;
- vi. the finite part of the virtual corrections computed in dimensional regularization;
- vii. the Born colour structures in the limit of a large number of colours.

The symmetric colour correlated \mathcal{B}_{ij} amplitudes, according to the particle labelling used in the POWHEG BOX ($q(1)\bar{q}'(2) \rightarrow W(3)b(4)\bar{b}(5)$), are given by

$$\mathcal{B}_{ii} = -C_F \mathcal{B}, \quad i = 1, 2, 4, 5 \quad (2.1)$$

$$\mathcal{B}_{12} = \left(C_F - \frac{C_A}{2}\right) \mathcal{B}, \quad \mathcal{B}_{14} = \left(2C_F - \frac{C_A}{2}\right) \mathcal{B}, \quad \mathcal{B}_{15} = -(2C_F - C_A) \mathcal{B}, \quad (2.2)$$

for the case where q is a quark. For the case where the first incoming particle is an antiquark, we have the same results with \mathcal{B}_{14} and \mathcal{B}_{15} exchanged. Here $C_A = 3$ and $C_F = 4/3$ are the Casimir invariants of the colour SU(3) representation. We have taken the squared Born amplitude \mathcal{B} from ref. [11] while the squared real amplitudes have been generated using MadGraph [39].

The assignment of colour flow for the two Feynman diagrams at the Born level is straightforward and unambiguous, and follows directly the propagation of quarks.

2.3 Validation of the NLO code

In the POWHEG BOX framework, it is possible to compute NLO distributions, taking advantage of the fact that the POWHEG BOX computes automatically all the counterterms needed to regularize the real distributions. It is then possible to check that, in the collinear and soft limits, the real amplitude has the correct behaviour, and that it is consistent with the Born cross section and the colour- and spin-correlated Born amplitudes.

The NLO distributions obtained within the POWHEG BOX, using a variant of the FKS subtraction scheme [40], have been checked against the codes developed in refs. [11, 12, 13] which use instead a phase-space slicing method with two cutoffs, to extract soft and collinear singularities analytically [41, 42, 43], as well as independent calculations of both virtual and real corrections, performed with several tools based on FORM [44], TRACER [45] and MAPLE codes. Full agreement has been found in all the studied distributions, assuring us that the ingredients provided to the POWHEG BOX are correct and consistent.

¹We notice that the $B^{\mu\nu}$ spin-correlated Born amplitudes are zero, since there are no external gluons at the Born level.

3. Theoretical introduction

In the POWHEG formalism, the generation of the hardest emission is performed first, at full NLO accuracy, and subsequent radiation is generated using shower Monte Carlo programs (see ref. [20] for a more detailed description of the method). In the following, we will briefly summarize a few features of the POWHEG method that will be useful in view of the discussion of sec. 3.4.

3.1 Generation of the underlying Born configuration

The first step of the generation process is the construction of the underlying Born kinematics, i.e. the generation of the Born momenta, distributed according to the function

$$\bar{B}(\Phi_n) = B(\Phi_n) + V(\Phi_n) + \int d\Phi_{\text{rad}} R(\Phi_{n+1}), \quad (3.1)$$

where B , V and R are the Born, virtual and real contributions to the NLO cross section, Φ_n specifies the kinematics of the underlying Born event with n final-state particles, Φ_{rad} are the radiation variables and the real-emission variables $\Phi_{n+1} \equiv \{\Phi_n, \Phi_{\text{rad}}\}$ are parametrized in terms of the underlying-Born and radiation ones.

3.2 Generation of the radiation variables

Once the momenta of the underlying Born have been generated, the POWHEG method proceeds to generate the radiation, i.e. Φ_{rad} , starting from the POWHEG cross section for the generation of the hardest emission

$$d\sigma = \bar{B}(\Phi_n) d\Phi_n \left\{ \Delta(\Phi_n, p_T^{\min}) + \Delta(\Phi_n, k_T(\Phi_{n+1})) \frac{R(\Phi_{n+1})}{B(\Phi_n)} d\Phi_{\text{rad}} \right\}, \quad (3.2)$$

where values of $k_T(\Phi_{n+1}) < p_T^{\min}$ are not allowed (here $p_T^{\min} \sim 1$ GeV, i.e. of the order of a typical hadronic scale). The Sudakov form factor Δ is given by

$$\Delta(\Phi_n, p_T) = \exp \left\{ - \int d\Phi_{\text{rad}} \frac{R(\Phi_{n+1})}{B(\Phi_n)} \theta(k_T(\Phi_{n+1}) - p_T) \right\}. \quad (3.3)$$

The function $k_T(\Phi_{n+1})$ should be equal, near the singular limit, to the transverse momentum of the emitted parton relative to the emitting one. The cross section in eq. (3.2) has the following properties:

- at large k_T it coincides with the NLO cross section up to next-to-next-to-leading order terms. In fact, in the large transverse-momentum region, eq. (3.2) can be written as

$$d\sigma = \bar{B}(\Phi_n) \frac{R(\Phi_{n+1})}{B(\Phi_n)} d\Phi_n d\Phi_{\text{rad}}, \quad (3.4)$$

since the Sudakov form factor approaches 1 in this region. This differs from the pure NLO result because of the presence of the factor

$$\frac{\bar{B}(\Phi_n)}{B(\Phi_n)} = 1 + \mathcal{O}(\alpha_s). \quad (3.5)$$

For processes that get large radiative corrections, the $\mathcal{O}(\alpha_s)$ term can be in fact of order 1, giving then a harder spectrum for the generated radiation.

- It reproduces correctly the value of infrared-safe observables at NLO. Thus, also its integral around the small k_T region has NLO accuracy.
- At small k_T it behaves no worse than standard shower Monte Carlo generators.

3.3 Tuning of the real contribution

In POWHEG it is possible to tune the contribution to the real cross section that is treated with the Monte Carlo shower technique. This was pointed out first in ref. [19], where the POWHEG method was formulated, and then implemented in the POWHEG BOX as a general feature. In this way, the enhancement in eq. (3.5) can be controlled, if necessary. In fact, the real cross section can be split into two positive contributions

$$R = R_s + R_f, \quad (3.6)$$

such that R_f has no singularities (soft or collinear) and only R_s is singular in the infrared regions. In previous implementations [22] the separation was achieved using a function F of the transverse momentum of the radiation, $0 \leq F \leq 1$, that approaches 1 when the transverse momentum of the radiated parton vanishes, and such that

$$R_s = R F, \quad (3.7)$$

$$R_f = R [1 - F]. \quad (3.8)$$

The generation of the radiation is then done by POWHEG using only the divergent contribution R_s and eqs. (3.2) and (3.3) become

$$d\sigma = \bar{B}_s(\Phi_n) d\Phi_n \left\{ \Delta_s(\Phi_n, p_T^{\min}) + \Delta_s(\Phi_n, k_T(\Phi_{n+1})) \frac{R_s(\Phi_{n+1})}{B(\Phi_n)} d\Phi_{\text{rad}} \right\} + R_f(\Phi_{n+1}) d\Phi_n d\Phi_{\text{rad}}, \quad (3.9)$$

$$\bar{B}_s(\Phi_n) = B(\Phi_n) + V(\Phi_n) + \int d\Phi_{\text{rad}} R_s(\Phi_{n+1}), \quad (3.10)$$

$$\Delta_s(\Phi_n, p_T) = \exp \left\{ - \int d\Phi_{\text{rad}} \frac{R_s(\Phi_{n+1})}{B(\Phi_n)} \theta(k_T(\Phi_{n+1}) - p_T) \right\}. \quad (3.11)$$

The contribution R_f , being finite and positive, is generated with standard NLO techniques, and fed into a shower Monte Carlo as is.

3.4 $Wb\bar{b}$ production

As for Higgs-boson production in gluon fusion [22], also in $Wb\bar{b}$ production the NLO corrections are very large, independently of the choice of the renormalization and factorization scale [11, 13]. For example, using a renormalization and factorization scale equal to $\mu = m_W + 2m_b$ and input parameters as specified in sec. 4, for $W^-b\bar{b}$ production at the LHC with $\sqrt{s} = 14$ TeV, the LO cross section corresponding to the distributions shown in

| m_b [GeV] | LO [pb] | NLO [pb] | K |
|-------------|---------------------|-------------------|-----|
| 0.1 | 140.6 ± 0.3 | 412 ± 8 | 2.9 |
| 1.0 | 135.5 ± 0.2 | 381 ± 2 | 2.8 |
| 10 | 37.11 ± 0.03 | 98.2 ± 0.3 | 2.6 |
| 100 | 0.5240 ± 0.0003 | 0.961 ± 0.003 | 1.8 |

Table 1: Values of the LO and NLO cross sections, as well as their respective K factors, for $W^- b\bar{b}$ production at the LHC with 14 TeV, using $\mu = m_W + 2m_b$ as renormalization and factorization scale and varying the quark mass m_b by three orders of magnitude.

fig. 2 is 81.32 pb, while the NLO cross section is 222.88 pb, with a K factor (ratio of NLO over LO total cross section) of 2.74, while at the Tevatron, the cross sections are 10.43 pb at LO, and 19.84 pb at NLO, with a K factor of 1.9.

We can attribute these large NLO corrections to at least two reasons: the opening of a new gluon-initiated channel in the real contributions at NLO (e.g. $qg \rightarrow Wb\bar{b} + q$), that is likely to be more important at the LHC than at the Tevatron [11, 12, 13], and the presence of large logarithms of the mass of the bottom quark, related to final-state collinear singularities for massless quarks, now regularized by the quark mass. To illustrate this, we have collected in table 1 the K factors for several values of the mass of the final-state heavy quark, for the LHC at 14 TeV, and using renormalization and factorization scales equal to $\mu = m_W + 2m_b$. One can see that the K factors are large and, when the quark mass increases from 0.1 GeV to 100 GeV, the K factor decreases from 2.9 to 1.8. We expect the large collinear logarithms to affect distributions even more than total cross sections.

Before presenting a few results for $Wb\bar{b}$ production, we would like to address a further issue related to this process: $Wb\bar{b}$ production has a Born zero when a relativistic W is emitted parallel with respect to the incoming beam, and consequently the gluon (which undergoes the splitting into a $b\bar{b}$ pair) is emitted in the opposite direction. Along the incoming beam, angular-momentum conservation cannot be preserved, and this configuration is kinematically suppressed. This was in fact the case for W production, where there is a zero in the Born cross section if the outgoing lepton from W decay is anti-parallel to the incoming quark [21]. In fact, due to the left-handed nature of the W boson coupling, we have a violation of angular-momentum conservation along the incoming beam.

Despite the fact that $B(\Phi_n^0)$ can vanish in some kinematic regions Φ_n^0 , this kinematics can be generated since the $\bar{B}_s(\Phi_n^0)$ term in eq. (3.10) can be different from zero, due to the real term. From eq. (3.9), we see that, in this case, away from the Sudakov region (i.e. where $\Delta_s \approx 1$), the real contribution may be enhanced by a factor \bar{B}_s/B , now large since $B \rightarrow 0$. The POWHEG BOX has a built-in mechanism to deal with this problem: R^s is chosen to vanish in the regions where R differs too much (by more than a factor of 5) from its collinear or soft approximation, which are proportional to the underlying Born cross section. The contribution $R_f = R - R_s$, being non-singular, is then added independently. To activate this mechanism, the POWHEG BOX flag `bornzerodamp` has to be set to 1. This must then necessarily be done for the process we are studying.

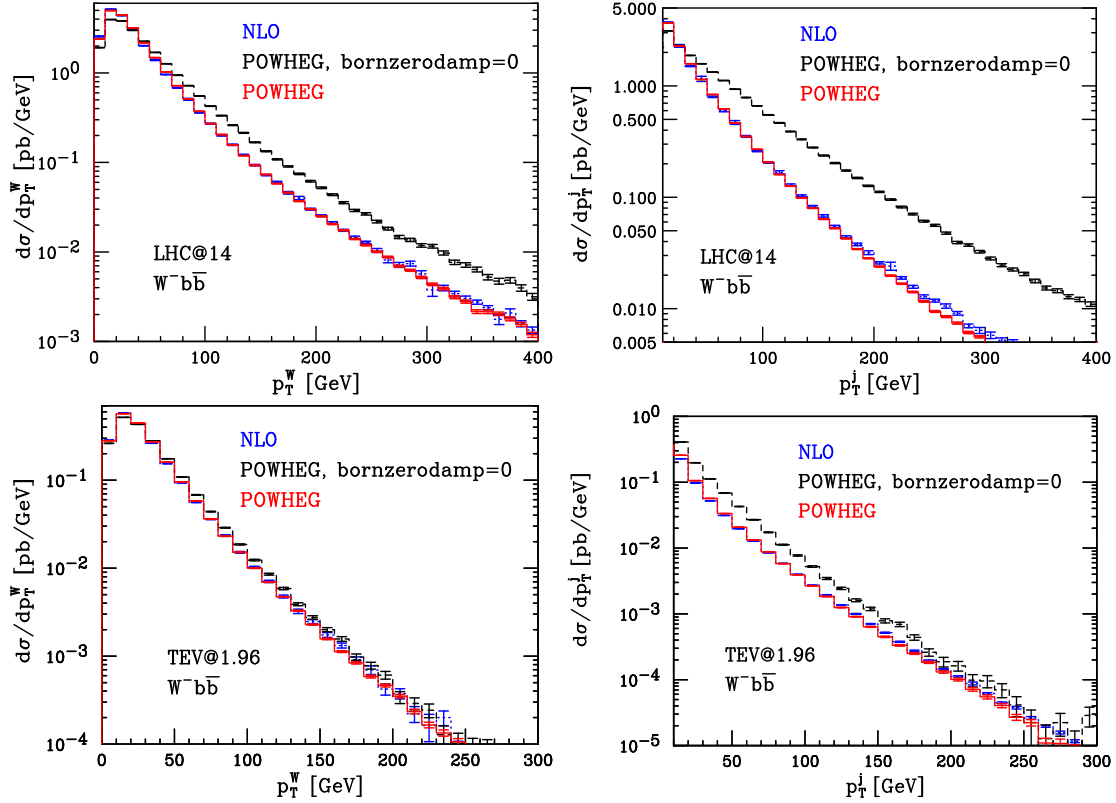


Figure 2: Transverse-momentum distributions for the W boson, p_T^W , and the hardest radiated non- b jet, p_T^j , in $W^-b\bar{b}$ production at NLO in QCD, for both the LHC with $\sqrt{s} = 14$ TeV (upper plots) and the Tevatron (lower plots). The dotted blue lines represent the results of the pure NLO QCD calculation. The POWHEG results obtained with the mechanism to protect from Born zero not activated and with no separation of the hard-radiation region are shown in dashed black lines. In solid red, the results with the mechanism to protect from Born zero activated and with the separation of the hard radiation collinear to the bottom quarks, as described in sec. 3.4.

In fig. 2, we have plotted the transverse momentum of the W boson and of the hardest radiated jet at the Tevatron and at the LHC. Jets are reconstructed using the anti- k_T algorithm [46] with $R = 0.4$, and jets are recombined using the default recombination E scheme [47]. No other cuts are applied to the events. The values of all the coupling constants, masses and physical parameters for the generation of these events can be found in sec. 4. In dashed black lines, the POWHEG hardest-emission results when the `bornzerodamp` flag is set to `false`. It is evident the effect of the enhancing factor \bar{B}_s/B with respect to the corresponding NLO results (dotted blue lines).

In addition to the activation of the mechanism to protect from the Born zeros, we have decided to separate out the region of hard-gluon emission collinear to one of the final-state massive quarks from the part of the real contribution that is treated by the Monte Carlo shower techniques (i.e. generated through the Sudakov form factor), and to handle it with standard NLO techniques, as described in sec. 3.3. In fact, this region is responsible for the

presence of large logarithms of the mass of the quark and we do not want these logarithmic terms to get further enhanced by the \bar{B}/B ratio of eq. (3.5). We would like to stress that, strictly speaking, this region is not singular, since the mass of the quark regularizes it, but it would be a singular region if the mass of the quark were exactly zero.

In order to separate out the region of hard-gluon emission collinear to the final-state b quarks, we have chosen the following form for the function F of eqs. (3.7) and (3.8)

$$F = \frac{(1/d)^c}{(1/d)^c + (1/d_b)^c + (1/d_{\bar{b}})^c}, \quad (3.12)$$

where

$$d = E^2 (1 - \cos^2 \theta), \quad (3.13)$$

$$d_b = \frac{E E_b}{(E + E_b)^2} \frac{(E + m_b)^2}{E^2} k \cdot k_b = E_b^2 \frac{(E + m_b)^2}{(E + E_b)^2} \left(1 - \frac{|\vec{k}_b|}{E_b} \cos \theta_b \right), \quad (3.14)$$

and where k is the momentum of the radiated gluon with energy E , forming an angle θ with the positive direction of the incoming beam, and an angle θ_b with the outgoing b quark, in the center-of-mass frame. The momentum of the b quark is k_b , with energy E_b and three-momentum \vec{k}_b . The $d_{\bar{b}}$ term is similar to the d_b one except for exchanging b with \bar{b} in all the kinematic variables. We have set $c = 1$ in the code, but higher values can be used too.

The function F in eq. (3.12) has the following properties:

1. it approaches 1 in the singular region, i.e. when the emitted gluon is parallel to the incoming beams or soft ($d \rightarrow 0$), assuring that the singular region is treated with the Monte Carlo shower technique;
2. it becomes small when the radiated parton is hard and collinear to the b or the \bar{b} quark. In fact, when the radiated gluon is hard and collinear to one of the two heavy quarks, the d_b or $d_{\bar{b}}$ terms reach their minimum value.

The distributions obtained with the mechanism to protect from the Born zeros and with the F function of eq. (3.12) are plotted as solid red lines in fig. 2. We find very good agreement with the NLO curves, at least in the region where we expect this to happen. The expected disagreement in the low- p_T jet region is due to the fact that the NLO curve is divergent in this region, while the resummed POWHEG result feels the effect of the Sudakov form factor and goes correctly to zero. In addition, we have verified that the major role in getting this agreement is played by the activation of the mechanism to protect from Born-zero configurations, while the effect of the separation of the region of hard gluons parallel to the massive b quarks plays only a minor role.

3.5 W -boson decay

Since we have used the analytic calculation of the virtual corrections of refs. [11, 12, 13], that treats the W boson as stable, we are not in a position to have all the spin correlations in

the leptonic W -boson decay products correctly accounted for. We can instead use standard techniques to implement the decay in an approximated way [37]. In this approximation, spin correlations are not accurate to NLO in the whole phase space, but are correct to NLO for hard real emissions and to leading order in the soft and collinear region. In order to achieve this, we have produced a W boson with invariant mass M distributed according to the Breit-Wigner function

$$\frac{1}{\pi} \frac{m_W \Gamma_W}{(M^2 - m_W^2) + m_W^2 \Gamma_W^2}, \quad (3.15)$$

where m_W and Γ_W are the pole mass and width of the W boson. Using the POWHEG method, a Born-like, or real-like event, is generated with an undecayed W boson, whose invariant mass is M , and whose kinematics is parametrized by a set of variables that we call Φ_u , where “u” stands for “undecayed”.

The procedure that we are going to follow can be easily illustrated if we recall that the squared matrix elements are connected to the concept of probability. We then rephrase the procedure that we have used in a probabilistic language. The differential probability distribution of the decay variables is proportional to (we neglect the overall normalization factor that ensures that the integral of the differential probability distribution is 1)

$$dP(\Phi_d) \div \mathcal{M}_d(\Phi_d) d\Phi_d = \mathcal{M}_d(\Phi_u, \Phi_{W \rightarrow l\nu}) d\Phi_u d\Phi_{W \rightarrow l\nu}, \quad (3.16)$$

where \mathcal{M}_d is the squared amplitude corresponding to the decayed process, with finite-width effects fully taken into account². For consistency, the squared amplitude \mathcal{M}_d must include only resonant diagrams (i.e. diagrams where the W momentum equals the sum of the l and ν momenta). In writing eq. (3.16), we have parametrized the kinematics of the process for the production and decay of the W boson in terms of the undecayed variables Φ_u and of a set of variables describing the W decay, $\Phi_{W \rightarrow l\nu}$. Equation (3.16) implicitly defines $d\Phi_{W \rightarrow l\nu}$. Similarly, the differential probability distribution of the undecayed variables is proportional to $\mathcal{M}_u(\Phi_u) d\Phi_u$. The problem is then to determine the probability distribution of the variables that parametrize the decay, $\Phi_{W \rightarrow l\nu}$, given the probability distributions for Φ_d and Φ_u . To solve this problem we use the fact that the joint probability of two events A and B can be written in terms of the conditional probability

$$P(A \cup B) = P(A|B) \times P(B), \quad (3.17)$$

that in our case becomes (A corresponds to the generation of the decay variables for $W \rightarrow l\nu$ and B corresponds to the generation of the undecayed $Wb\bar{b}$ event)

$$\mathcal{M}_d(\Phi_d) d\Phi_d \div dP(\Phi_{W \rightarrow l\nu} | \Phi_u) \times \mathcal{M}_u(\Phi_u) d\Phi_u, \quad (3.18)$$

²The decayed tree-level squared amplitudes \mathcal{M}_d have been obtained using MadGraph [39], both for the Born and for the radiative processes.

where $dP(\Phi_{W \rightarrow l\nu} | \Phi_u)$ is the infinitesimal probability distribution of the variables $\Phi_{W \rightarrow l\nu}$, given the kinematics of an undecayed process Φ_u . We can then write, using eq. (3.16),

$$\begin{aligned} dP(\Phi_{W \rightarrow l\nu} | \Phi_u) &\div \frac{\mathcal{M}_d(\Phi_d) d\Phi_d}{\mathcal{M}_u(\Phi_u) d\Phi_u} = \frac{\mathcal{M}_d(\Phi_u, \Phi_{W \rightarrow l\nu}) d\Phi_u d\Phi_{W \rightarrow l\nu}}{\mathcal{M}_u(\Phi_u) d\Phi_u} \\ &= \frac{\mathcal{M}_d(\Phi_u, \Phi_{W \rightarrow l\nu})}{\mathcal{M}_u(\Phi_u)} d\Phi_{W \rightarrow l\nu}. \end{aligned} \quad (3.19)$$

$dP(\Phi_{W \rightarrow l\nu} | \Phi_u)/d\Phi_{W \rightarrow l\nu}$ is the distribution function we are looking for. To generate efficiently $\Phi_{W \rightarrow l\nu}$, distributed according to (3.19), we use the hit-and-miss technique and so we need to find an upper bound for the ratio $\mathcal{M}_d(\Phi_u, \Phi_{W \rightarrow l\nu})/\mathcal{M}_u(\Phi_u)$. We have used as upper bounding function the expression

$$U_d(M^2, \Phi_{W \rightarrow l\nu}) = N_d \frac{2M^2 + m_l^2}{(M^2 - m_W^2)^2 + m_W^2 \Gamma_W^2} \mathcal{M}_{W \rightarrow l\nu}(M^2), \quad (3.20)$$

where N_d is a normalization factor, $\mathcal{M}_{W \rightarrow l\nu}$ is the squared decay amplitude corresponding to the $W \rightarrow l\nu$ decay and m_l is the charged-lepton mass. One can predict the appropriate value for the normalization factor N_d or compute it by sampling the decay phase space $\Phi_{W \rightarrow l\nu}$ and comparing U_d with the exact expression, in such a way that the inequality

$$\frac{\mathcal{M}_d(\Phi_u, \Phi_{W \rightarrow l\nu})}{\mathcal{M}_u(\Phi_u)} \leq U_d(M^2, \Phi_{W \rightarrow l\nu}) \quad (3.21)$$

holds. The veto algorithm is then applied as follows:

1. first one generates a point in the phase space $\Phi_{W \rightarrow l\nu}$;
2. then a random number r in the range $[0, U_d(M^2, \Phi_{W \rightarrow l\nu})]$ is generated;
3. finally, if $r < \mathcal{M}_d(\Phi_u, \Phi_{W \rightarrow l\nu})/\mathcal{M}_u(\Phi_u)$, the kinematics of the decay is kept and the event is generated. Otherwise the algorithm goes back to step 1.

At the end of this procedure, the kinematics $\Phi_{W \rightarrow l\nu}$ of the W decay is generated, and, together with the POWHEG-generated undecayed variables Φ_u , the kinematics of $Wb\bar{b}$ event followed by the decay of the W boson becomes available.

In fig. 3 we have plotted the differential cross section as a function of the transverse momentum of the charged lepton p_T^l and its pseudorapidity η^l , generated with the procedure described above, in solid red lines. For comparison we have plotted, in dashed blue lines, the NLO differential cross section for $W^- b\bar{b} \rightarrow l^- \bar{\nu} b\bar{b}$ production of ref. [14], as implemented in MCFM 6.0 [48], where spin correlations of the decay products have been included exactly. The branching ratio applied to the POWHEG hardest-emission results has been taken from the ratio

$$\text{BR}(W \rightarrow l\nu) = \frac{\sigma_{\text{LO, MCFM}}}{\sigma_{\text{LO, POWHEG}}} = 0.103. \quad (3.22)$$

As can be seen from the insert in the lower part of the two plots, where we have plotted the ratio of the POWHEG hardest emission results over the exact NLO ones (PW/NLO), the approximated decay distributions are in very good agreement with the exact ones.

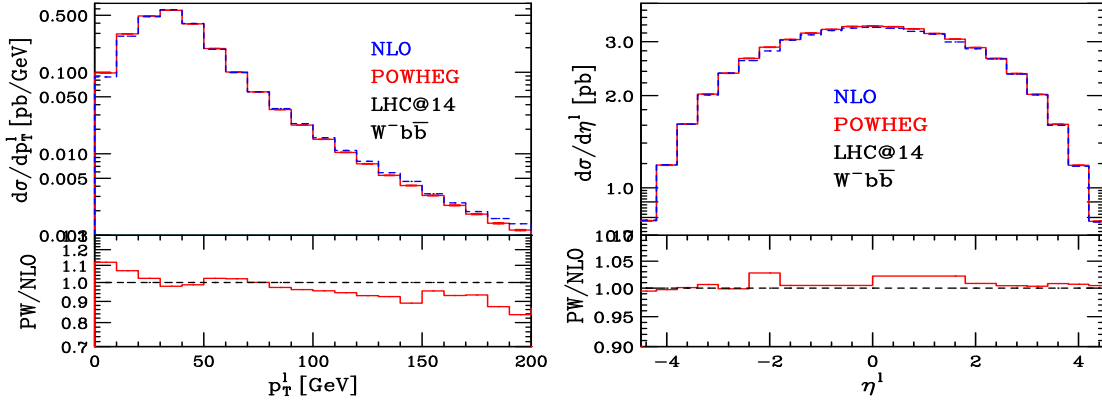


Figure 3: Transverse momentum, p_T^l , and pseudorapidity, η^l , distributions for the final-state lepton produced in $W^- b\bar{b} \rightarrow l^- \bar{\nu} b\bar{b}$, at the LHC with $\sqrt{s} = 14$ TeV. The distributions generated by the POWHEG BOX according to the method described in sec. 3.5 are shown in solid red lines, while the NLO results computed with the MCFM code are shown in dashed blue lines. The lower inserts show the ratio between the two distributions: POWHEG/NLO.

4. Phenomenology

In this section we present a few results for $W^- b\bar{b} \rightarrow l^- \bar{\nu} b\bar{b}$ production at the Tevatron and at the LHC. Similar results can be obtained for $W^+ b\bar{b} \rightarrow l^+ \nu b\bar{b}$.

For future reference, we list here the values of all the parameters and physical quantities that enter the calculation:

$$\begin{aligned} m_W &= 80.41 \text{ GeV}, & m_b &= 4.62 \text{ GeV}, & m_t &= 173.1 \text{ GeV}, \\ \Gamma_W &= 2.141 \text{ GeV}, & \text{BR}(W \rightarrow l\nu) &= 0.103, \end{aligned} \quad (4.1)$$

and

$$\sin^2 \theta_W = 0.223, \quad \alpha = 1/132.088832, \quad G_F = 1.16639 \times 10^{-5} \text{ GeV}^{-2}, \quad (4.2)$$

from which we derive ($g_W^2 = 8m_W^2 G_F / \sqrt{2}$)

$$g_W = 0.6532. \quad (4.3)$$

We have used the CTEQ6.6 pdf set [49], and we have set the renormalization and factorization scale to the fixed value

$$\mu = m_W + 2m_b, \quad (4.4)$$

from which we compute the two-loop $\overline{\text{MS}}$ strong coupling constant $\alpha_s(\mu) = 0.1183$ with 5 light flavors. The W -boson couplings to quarks are proportional to the Cabibbo-Kobayashi-Maskawa (CKM) matrix elements. We use non-zero CKM matrix elements for the first two quark generations, $V_{ud} = V_{cs} = 0.974$ and $V_{us} = V_{cd} = 0.227$, while we neglect the contribution of the third generation, since it is suppressed either by the initial-state quark pdfs or by the corresponding CKM matrix elements.

Jets are defined using the anti- k_T algorithm [46] with $R = 0.4$ and $k_{T\min} = 5$ GeV, and are recombined using the default E scheme.

Since there are no data for W plus two b jets to compare our predictions with, and consequently no experimental analysis is available, we have chosen a set of cuts that, while reasonable, are less stringent than the experimental ones. In fact, the purpose of this section is to show the differences between several POWHEG results, obtained with different showering programs, rather than provide predictions for experimentalists, who can use the POWHEG BOX by themselves to generate events and analyze them according to their experimental selection criteria.

The set of cuts for the Tevatron, $\sqrt{s} = 1.96$ TeV, and the LHC, $\sqrt{s} = 14$ TeV, are the following:

$$\begin{aligned} p_T^b &> 15 \text{ GeV}, & |\eta^b| < 3, & p_T^j > 15 \text{ GeV}, & |y^j| < 3, \\ p_T^l &> 15 \text{ GeV}, & |\eta^l| < 3, & \cancel{E}_T > 15 \text{ GeV}. \end{aligned} \quad (4.5)$$

We keep only events with at least two b -jets that pass the cuts on the transverse momentum p_T^b and on the pseudorapidity η^b , disregarding all the other events. Non- b jets are required to have a minimum transverse momentum of 15 GeV and to be in the rapidity region $|y^j| < 3$. Since we have decayed the W boson, we have cuts on the transverse momentum p_T^l and pseudorapidity η^l of the charged lepton, and a cut on the missing energy \cancel{E}_T , due to the presence of the undetected neutrino.

In the following, we present several kinematic distributions both for the Tevatron and the LHC, and we plot results for the hardest-emission POWHEG cross section with no shower (dotted black lines), and for the same results showered by PYTHIA (red solid curves) and HERWIG (dashed blue lines). We have run PYTHIA with the Perugia 0 tuning, switching off multi-particle interactions³, in order to make a fair comparison with HERWIG, that uses the separate package JIMMY [50] to generate multi-particle interactions. We have run HERWIG in its default configuration, with intrinsic p_T -spreading of 2.5 GeV.

Our analysis is based on a sample of 29 million events for the Tevatron and 26 million events for the LHC, generated with the POWHEG BOX with no folding (see ref. [36] for more details). For the Tevatron we got a 15% fraction of negative-weight events and 12% for the LHC, that we have kept in our analysis. If one is interested in the generation of only

| ξ | y | ϕ | negative fraction (%) | ξ | y | ϕ | negative fraction (%) |
|-------|-----|--------|-----------------------|-------|-----|--------|-----------------------|
| 1 | 1 | 1 | 12 | 2 | 5 | 10 | 2.3 |
| 1 | 1 | 10 | 8 | 5 | 5 | 5 | 1.8 |
| 1 | 10 | 2 | 7 | 5 | 5 | 10 | 1.5 |
| 10 | 1 | 5 | 5 | 10 | 10 | 10 | 0.9 |

Table 2: Negative-weight fractions as a function of the folding in the radiation variables $\Phi_{\text{rad}} = \{\xi, y, \phi\}$, at the LHC.

positive-weight events, then the foldings of the radiation variables ($\Phi_{\text{rad}} = \{\xi, y, \phi\}$) should

³We have set `mstp(81)=20` in the code, after the call to `pytune`.

be increased. We have collected in table 2 a few results for different values of the foldings in the ξ , y and ϕ variables. From the table it is evident that, as the product of the folding numbers increases, the fraction of negative-weight events gets smaller and smaller, but at the price of a decrease in the speed of the code.

4.1 Tevatron results

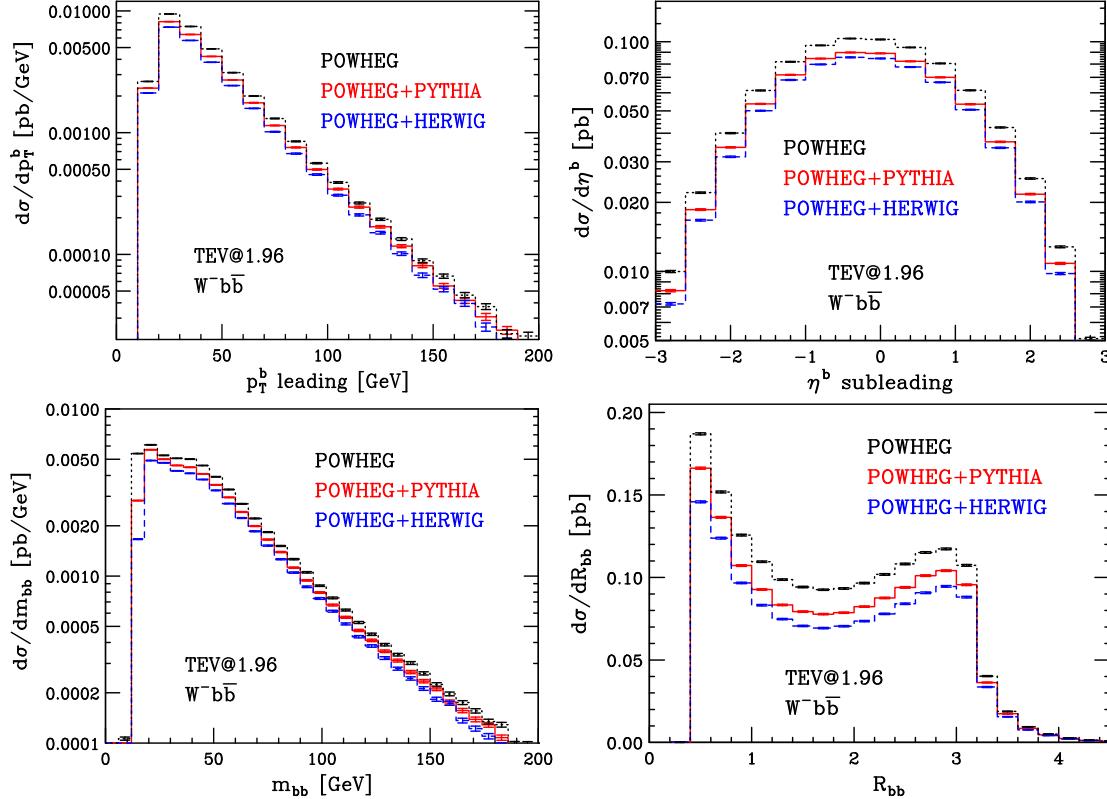


Figure 4: Differential cross sections as a function of the transverse momentum of the hardest b jet, p_T^b leading, the pseudorapidity of the second hardest b jet, η^b subleading, the invariant mass of the leading and subleading b jets, m_{bb} , and their angular distance R_{bb} , for $W^- b\bar{b} \rightarrow l^- \bar{\nu} b\bar{b}$ production at the Tevatron. The different curves represent the results for the POWHEG hardest emission (dotted black), and for POWHEG interfaced with either PYTHIA (solid red) or HERWIG (dashed blue).

In fig. 4 we have plotted the differential cross sections as a function of the transverse momentum of the b jet with the hardest p_T (called leading b jet), of the pseudorapidity of the b jet with the second hardest transverse momentum (called subleading b jet), of the invariant mass of the leading and subleading b jets and of the angular distribution R_{bb} , defined as

$$R_{bb} = \sqrt{\Delta y_{bb}^2 + \Delta \phi_{bb}^2}, \quad (4.6)$$

where Δy_{bb} and $\Delta \phi_{bb}$ are the difference in the rapidities and in the azimuthal angles of the two highest- p_T b jets. Error bars from the Monte Carlo generator are shown too.

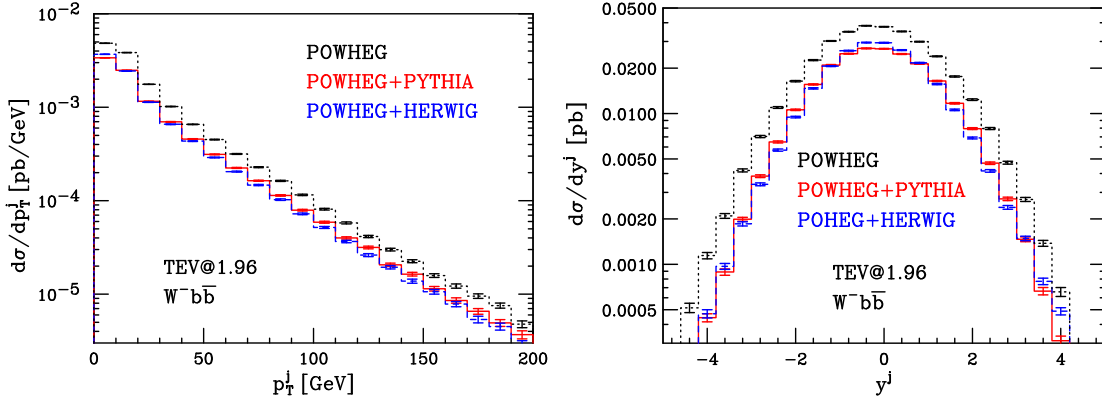


Figure 5: Differential cross sections as a function of the transverse momentum, p_T^j , and the rapidity, y^j , of the hardest radiated non- b jet, for $W^- b\bar{b} \rightarrow l^- \bar{\nu} b\bar{b}$ production at the Tevatron. The different curves represent the results for the POWHEG hardest emission (dotted black), and for POWHEG interfaced with either PYTHIA (solid red) or HERWIG (dashed blue).

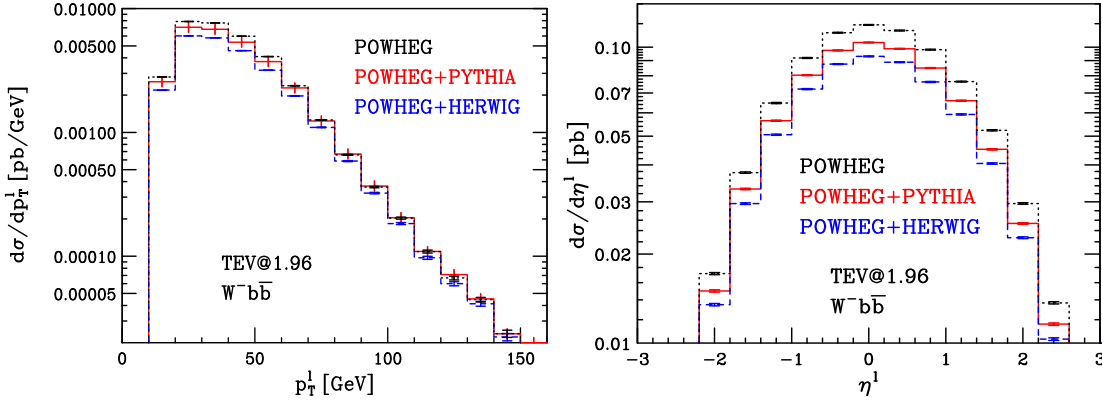


Figure 6: Differential cross sections as a function of the transverse momentum, p_T^l , and the pseudorapidity, η^l , of the lepton for $W^- b\bar{b} \rightarrow l^- \bar{\nu} b\bar{b}$ production at the Tevatron. The different curves represent the results for the POWHEG hardest emission (dotted black), and for POWHEG interfaced with either PYTHIA (solid red) or HERWIG (dashed blue).

In fig. 5, we have plotted the differential cross sections as a function of the transverse momentum of the hardest radiated (non- b) jet, p_T^j , and its rapidity y^j , while in fig. 6 we have plotted the cross sections as a function of the transverse momentum p_T^l and pseudorapidity η^l of the hardest charged lepton. Finally, in fig. 7, we show the differential cross sections as a function of $(y^{Wb\bar{b}} - y^j)$, i.e. the difference between the rapidity of the $Wb\bar{b}$ system (the W momentum is taken from the showering program, since the neutrino goes undetected) and the rapidity of the hardest jet, and as a function of the difference in the azimuthal angles of the two b jets, $\Delta\phi_{bb}$.

In all the plots, we can see that the different showers implemented by PYTHIA and HERWIG give slightly different distributions, and we can consider this difference as a the-

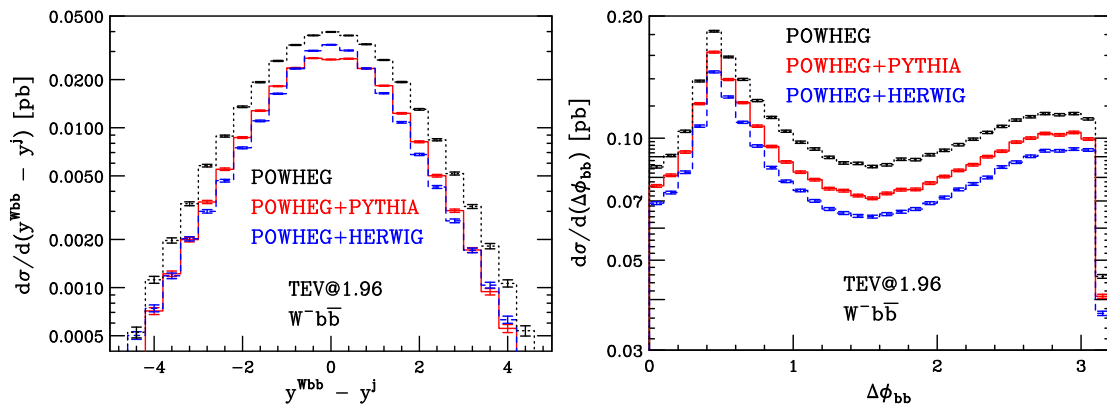


Figure 7: Differential cross sections as a function of the rapidity difference between the $Wb\bar{b}$ system and the hardest radiated non- b jet, $(y^{Wbb} - y^j)$, and the azimuthal angle difference between the two b jets $\Delta\phi_{bb}$, for $W^- b\bar{b} \rightarrow l^- \bar{\nu} b\bar{b}$ production at the Tevatron. The different curves represent the results for the POWHEG hardest emission (dotted black), and for POWHEG interfaced with either PYTHIA (solid red) or HERWIG (dashed blue).

oretical error associated to showering effects. The trend of the distributions is the same in all the plots: the differential cross sections from POWHEG followed by the shower done by PYTHIA (POWHEG+PYTHIA) are slightly larger than the corresponding ones showered by HERWIG (POWHEG+HERWIG). A consequence of this fact is that the cross sections, after the cuts of eq. (4.5), are given by

$$\sigma_{\text{POWHEG}} = 0.335 \text{ pb}, \quad \sigma_{\text{POWHEG+PYTHIA}} = 0.291 \text{ pb}, \quad \sigma_{\text{POWHEG+HERWIG}} = 0.262 \text{ pb}. \quad (4.7)$$

In order to evidenciate the differences between the POWHEG (PW), the POWHEG+PYTHIA (PW+PY) and the POWHEG+HERWIG (PW+HW) results, in fig. 8 we have plotted their ratio for a sample of distributions. While the ratios of the POWHEG hardest emission cross sections over the POWHEG showered results (PW/(PW+PY) for the shower done by PYTHIA, in dashed red lines, and PW/(PW+HW) for the shower done by HERWIG, in dotted blue lines) are just an indication of the effect of the completion of the shower on the POWHEG hardest-emission events, the ratios (PW+PY)/(PW+HW) carry information on the effects of the two different showering algorithms implemented in PYTHIA and HERWIG. As can be inferred from the (PW+PY)/(PW+HW) ratios in the figures, these effects amount to differences of the order of 10–20%, and this can be taken as the theoretical errors connected with using different showering programs. In general, the ratios are almost flat. The only distribution that shows some phase-space dependence is the rapidity of the hardest jet, in the lower left plot of fig. 8, corresponding to the ratios of the curves in the right-hand-side plot in fig. 5. Here, PW+HW jets tend to be more central in rapidity then the PW+PY ones. We expect this same behaviour to be present in fig. 7 as well, since we are plotting the differential distribution as a function of $(y^{Wbb} - y^j)$, and the rapidity of the jet enters directly in this quantity.

4.2 LHC results

In figs. 9, 10, 11 and 12, we have plotted the same differential cross sections we have

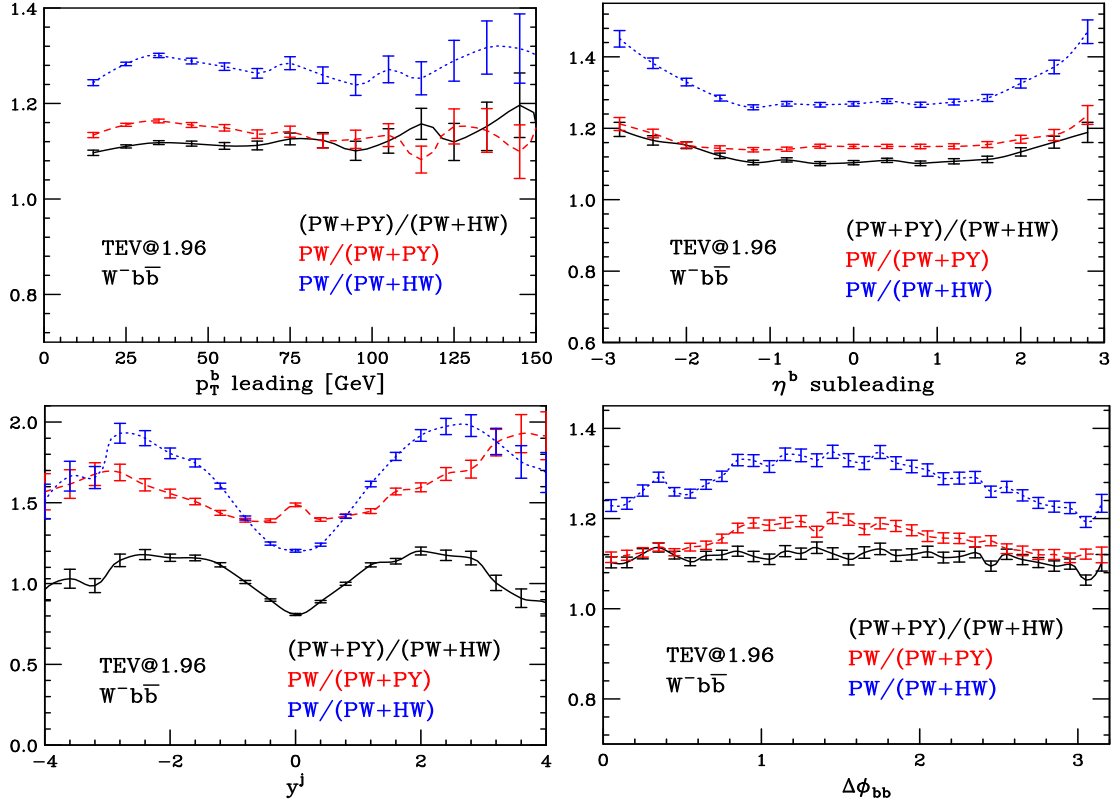


Figure 8: Ratios of the differential cross sections for $W^- b \bar{b} \rightarrow l^- \bar{\nu} b \bar{b}$ production at the Tevatron: (POWHEG+PYTHIA)/ (POWHEG+HERWIG) in solid black lines, POWHEG/(POWHEG+PYTHIA) in dashed red lines and POWHEG/(POWHEG+HERWIG) in dotted blue lines. Starting from the upper left corner and moving clockwise we show the ratio of the differential cross sections as function of the transverse momentum of the hardest b jet, p_T^b leading, the pseudorapidity of the second hardest b jet, η^b subleading, the azimuthal angular difference between the two b jets, $\Delta\phi_{bb}$, and the rapidity of the hardest radiated non b jet, y^j .

studied for the Tevatron, this time for the LHC with $\sqrt{s} = 14$ TeV. The behaviour of all the distributions is the same as for the Tevatron, and the corresponding cross sections after cuts are given by

$$\sigma_{\text{POWHEG}} = 3.08 \text{ pb}, \quad \sigma_{\text{POWHEG+PYTHIA}} = 2.83 \text{ pb}, \quad \sigma_{\text{POWHEG+HERWIG}} = 2.68 \text{ pb}. \quad (4.8)$$

In fig. 13, we have plotted the ratios (PW+PY)/(PW+HW) in solid black lines, PW/(PW+PY) in dashed red lines and PW/(PW+HW) in dotted blue lines. The effects of the two different showers, i.e. the ratios (PW+PY)/(PW+HW) are of the order of less than 10% for most of the distributions considered, so that the differences between the two showering algorithms is less pronounced at the LHC than at the Tevatron. Again, the distribution that turns out to be more sensitive to the showering procedure is the rapidity of the hardest jet, as illustrated in the lower left-hand-side plot of the figure, where jets from the HERWIG shower tend to be more central in rapidity than jets from the PYTHIA shower.

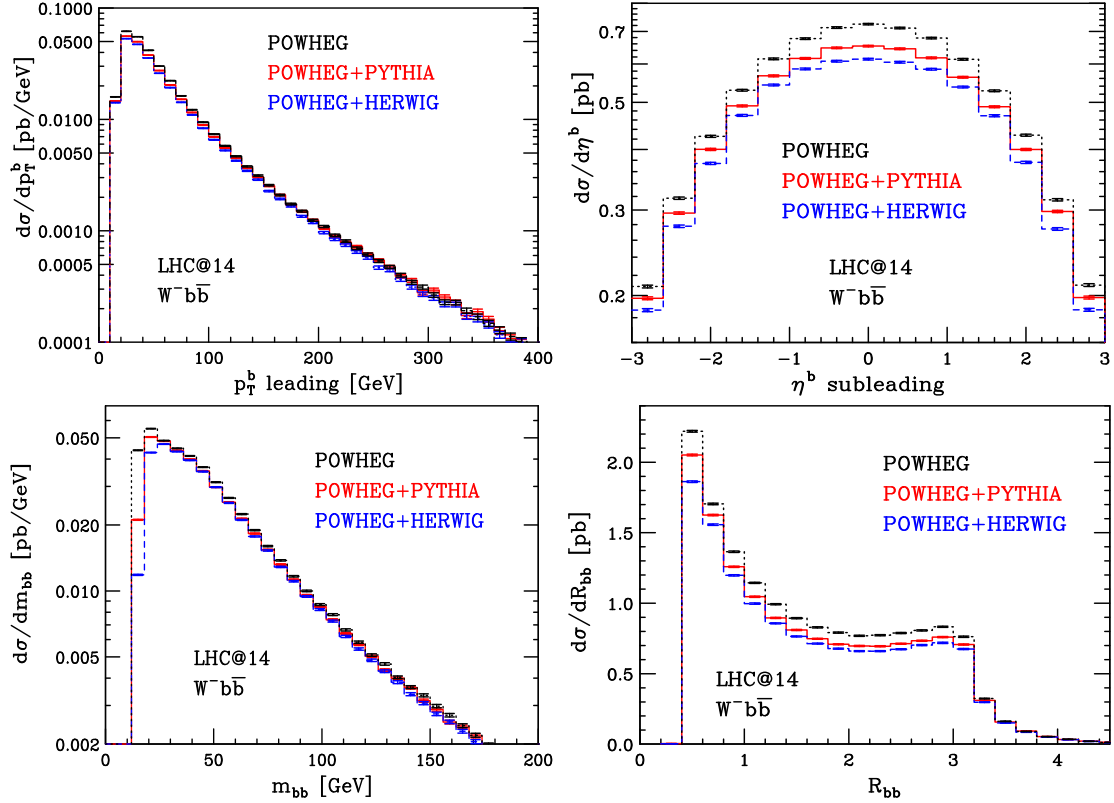


Figure 9: Differential cross section as a function of the transverse momentum of the hardest b jet, p_T^b leading, the pseudorapidity of the second hardest b jet, η^b subleading, the invariant mass of the leading and subleading b jets m_{bb} , and their angular distance R_{bb} , for $W^- b\bar{b} \rightarrow l^- \bar{\nu} b\bar{b}$ production at the LHC with $\sqrt{s} = 14$ TeV. The different curves represent the results of POWHEG hardest emission (dotted black), and of POWHEG interfaced with either PYTHIA (solid red) or HERWIG (dashed blue).

5. Conclusions

In this article we have presented a next-to-leading order plus parton shower simulation of the production of a W boson in association with a massive $b\bar{b}$ pair, based on the POWHEG formalism, with the leptonic decay of the W boson taken into account using standard approximated techniques. We have assembled our generator with the aid of the POWHEG BOX toolkit [36]. The NLO virtual corrections have been taken from [11, 12, 13] and their validity has been expanded in order to account for the case of an off-shell W boson production.

We have validated the code after taking care of activating the POWHEG BOX mechanism to protect from Born-zero configurations, and after separating out from the part of the real-radiation contribution treated with Monte Carlo techniques the region of hard gluons collinear to the final-state massive b quarks, to be treated with standard NLO techniques. This was done to prevent the enhancement of mass logarithmic terms by the POWHEG factor \bar{B}/B .

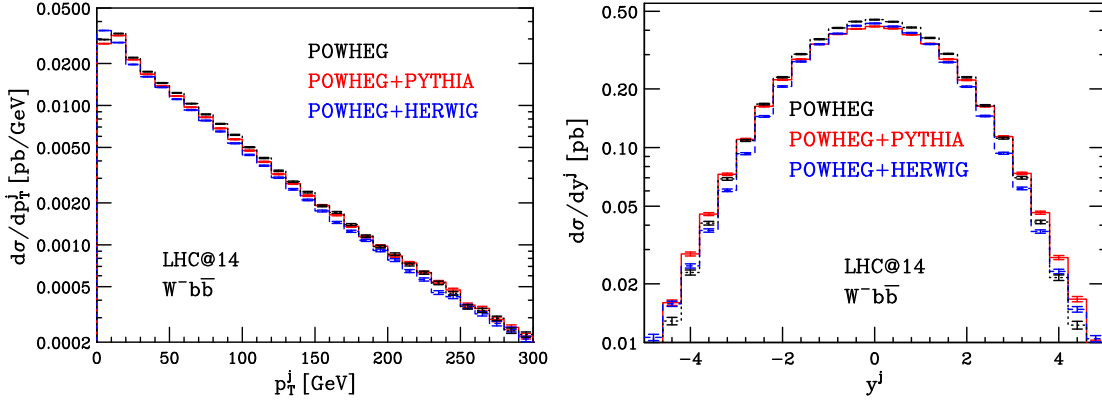


Figure 10: Differential cross section as a function of the transverse momentum, p_T^j , and the rapidity y^j of the hardest radiated non- b jet, for $W^- b\bar{b} \rightarrow l^- \bar{\nu} b\bar{b}$ production at the LHC with $\sqrt{s} = 14$ TeV. The different curves represent the results of POWHEG hardest emission (dotted black), and of POWHEG interfaced with either PYTHIA (solid red) or HERWIG (dashed blue).

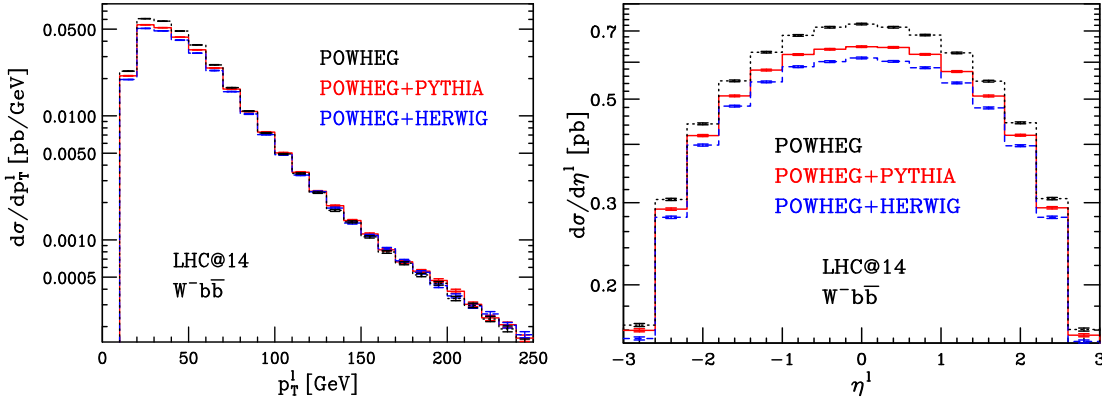


Figure 11: Differential cross section as a function of the transverse momentum, p_T^l , and the pseudorapidity η^l of the lepton for $W^- b\bar{b} \rightarrow l^- \bar{\nu} b\bar{b}$ production at the LHC with $\sqrt{s} = 14$ TeV. The different curves represent the results of POWHEG hardest emission (dotted black), and of POWHEG interfaced with either PYTHIA (solid red) or HERWIG (dashed blue).

Finally, we have showered the hardest-emission results generated by POWHEG with two popular shower Monte Carlo programs: PYTHIA and HERWIG. Looking at various kinematic distributions, we have found discrepancies of the order of 10–20% for the Tevatron and of less than 10% for the LHC between the two shower Monte Carlo programs. Discrepancies larger than the quoted values can be found in distributions involving the rapidity of the hardest radiated jet. These discrepancies can be considered as theoretical errors associated with the two different showering algorithms.

The tool we provide will be very important for both Higgs-boson and beyond the Standard Model searches at both the Tevatron and the LHC. Indeed $W + b$ jets is one of the main backgrounds to these searches and $Wb\bar{b}$ production is the main contribution.

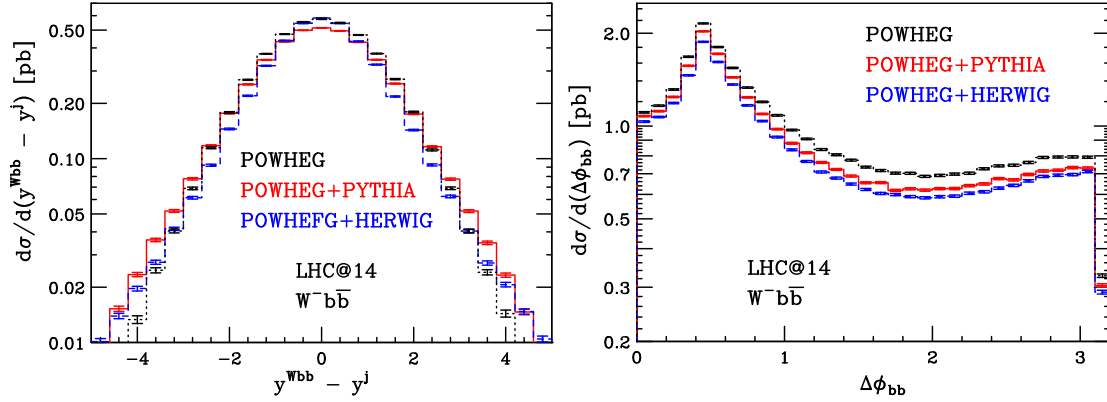


Figure 12: Differential cross section as a function of the rapidity difference between the $Wb\bar{b}$ system and the hardest radiated non- b jet, $(y^{Wbb} - y^j)$, and the azimuthal angle difference between the two b jets $\Delta\phi_{bb}$, for $W^- b\bar{b} \rightarrow l^- \bar{\nu} b\bar{b}$ production at the LHC with $\sqrt{s} = 14$ TeV. The different curves represent the results of POWHEG hardest emission (dotted black), and of POWHEG interfaced with either PYTHIA (solid red) or HERWIG (dashed blue).

The code of our generator can be accessed in the POWHEG BOX svn repository

`svn://powhegbox.mib.infn.it/trunk/POWHEG-BOX,`

with username `anonymous` and password `anonymous`.

Acknowledgments

We wish to thank P. Nason and F. Febres Cordero for useful discussions and we acknowledge the use of the Turing cluster of the INFN group IV in the Theory Division of the Physics Department at the University of Milano-Bicocca. We thank E. Re for carefully reading the paper. The work of L.R. is supported in part by the U.S. Department of Energy under grant DE-FG02-97IR41022.

References

- [1] **CDF** Collaboration, T. Aaltonen *et. al.*, *First Measurement of the b -jet Cross Section in Events with a W Boson in $p\bar{p}$ Collisions at $\sqrt{s} = 1.96$ TeV*, *Phys. Rev. Lett.* **104** (2010) 131801, [[arXiv:0909.1505](#)].
- [2] **D0** Collaboration, V. M. Abazov *et. al.*, *A search for $Wb\bar{b}$ and WH production in $p\bar{p}$ collisions at $\sqrt{s} = 1.96$ TeV*, *Phys. Rev. Lett.* **94** (2005) 091802, [[hep-ex/0410062](#)].
- [3] G. Piacquadio, *Identification of b -jets and investigation of the discovery potential of a Higgs boson in the $WH \rightarrow l\nu b\bar{b}$ channel with the ATLAS experiment*, *CERN-THESIS-2010-027*.
- [4] J. M. Butterworth, A. R. Davison, M. Rubin, and G. P. Salam, *Jet substructure as a new Higgs search channel at the LHC*, *Phys. Rev. Lett.* **100** (2008) 242001, [[arXiv:0802.2470](#)].
- [5] ATLAS Collaboration, , *Tech. Rep. ATL-PHYS-INT-2009-068, ATL-PHYS-PUB-2009-088*, CERN, Geneva, June, 2009.

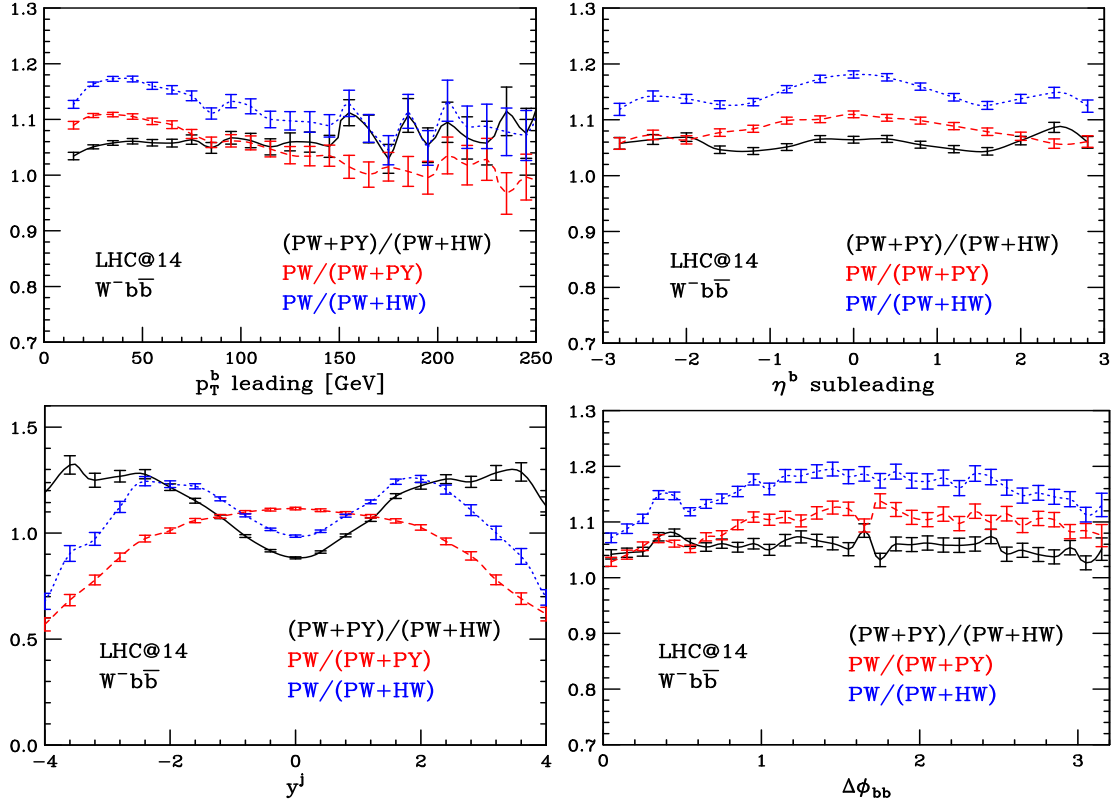


Figure 13: Ratios of the differential cross sections for $W^- b\bar{b} \rightarrow l^- \bar{\nu} b\bar{b}$ production at the LHC: (POWHEG+PYTHIA)/ (POWHEG+HERWIG) in solid black lines, POWHEG/(POWHEG+PYTHIA) in dashed red lines and POWHEG/(POWHEG+HERWIG) in dotted blue lines. Starting from the upper left corner and moving clockwise we show the ratio of the differential cross sections as function of the transverse momentum of the hardest b jet, p_T^b leading, the pseudorapidity of the second hardest b jet, η^b subleading, the azimuthal angular difference between the two b jets, $\Delta\phi_{bb}$, and the rapidity of the hardest radiated non b jet, y^j .

- [6] J. Campbell, R. K. Ellis, F. Maltoni, and S. Willenbrock, *Production of a W boson and two jets with one b-quark tag*, *Phys. Rev.* **D75** (2007) 054015, [[hep-ph/0611348](#)].
- [7] Z. Bern, L. J. Dixon, and D. A. Kosower, *One-loop amplitudes for e^+e^- to four partons*, *Nucl. Phys.* **B513** (1998) 3–86, [[hep-ph/9708239](#)].
- [8] Z. Bern, L. J. Dixon, D. A. Kosower, and S. Weinzierl, *One-loop amplitudes for $e^+e^- \rightarrow q\bar{q}Q\bar{Q}$* , *Nucl. Phys.* **B489** (1997) 3–23, [[hep-ph/9610370](#)].
- [9] R. K. Ellis and S. Veseli, *Strong radiative corrections to $Wb\bar{b}$ production in $p\bar{p}$ collisions*, *Phys. Rev.* **D60** (1999) 011501, [[hep-ph/9810489](#)].
- [10] J. M. Campbell and R. K. Ellis, *Next-to-leading order corrections to $W + 2$ jet and $Z + 2$ jet production at hadron colliders*, *Phys. Rev.* **D65** (2002) 113007, [[hep-ph/0202176](#)].
- [11] F. Febres Cordero, L. Reina, and D. Wackerroth, *NLO QCD corrections to W boson production with a massive b-quark jet pair at the Tevatron $p\bar{p}$ collider*, *Phys. Rev.* **D74** (2006) 034007, [[hep-ph/0606102](#)].

- [12] F. Febres Cordero, *Next-to-Leading-Order Corrections to Weak Boson Production with a Massive Quark Jet Pair at Hadron Colliders*, 0809.3829.
- [13] F. Febres Cordero, L. Reina, and D. Wackeroth, *W- and Z-boson production with a massive bottom-quark pair at the Large Hadron Collider*, *Phys. Rev.* **D80** (2009) 034015, [[arXiv:0906.1923](#)].
- [14] S. Badger, J. M. Campbell, and R. K. Ellis, *QCD corrections to the hadronic production of a heavy quark pair and a W-boson including decay correlations*, *JHEP* **03** (2011) 027, [[arXiv:1011.6647](#)].
- [15] J. Campbell, R. K. Ellis, F. Febres Cordero, F. Maltoni, L. Reina, D. Wackeroth, and S. Willenbrock, *Associated production of a W boson and one b jet*, *Phys. Rev.* **D79** (2009) 034023, [0809.3003].
- [16] F. F. Cordero, *Jet and W/Z Production at Hadron Colliders*, *PoS HCP2009* (2009) 008, [[arXiv:1001.2954](#)].
- [17] F. F. Cordero, L. Reina, and D. Wackeroth, *Associated production of a W or Z boson with bottom quarks at the Tevatron and the LHC*, *PoS RADCOR2009* (2010) 055, [[arXiv:1001.3362](#)].
- [18] S. Frixione and B. R. Webber, *Matching NLO QCD computations and parton shower simulations*, *JHEP* **06** (2002) 029, [[hep-ph/0204244](#)].
- [19] P. Nason, *A new method for combining NLO QCD with shower Monte Carlo algorithms*, *JHEP* **11** (2004) 040, [[hep-ph/0409146](#)].
- [20] S. Frixione, P. Nason, and C. Oleari, *Matching NLO QCD computations with Parton Shower simulations: the POWHEG method*, *JHEP* **11** (2007) 070, [[arXiv:0709.2092](#)].
- [21] S. Alioli, P. Nason, C. Oleari, and E. Re, *NLO vector-boson production matched with shower in POWHEG*, *JHEP* **07** (2008) 060, [[arXiv:0805.4802](#)].
- [22] S. Alioli, P. Nason, C. Oleari, and E. Re, *NLO Higgs boson production via gluon fusion matched with shower in POWHEG*, *JHEP* **04** (2009) 002, [[arXiv:0812.0578](#)].
- [23] P. Nason and C. Oleari, *NLO Higgs boson production via vector-boson fusion matched with shower in POWHEG*, *JHEP* **02** (2010) 037, [[arXiv:0911.5299](#)].
- [24] S. Alioli, P. Nason, C. Oleari, and E. Re, *NLO single-top production matched with shower in POWHEG: s- and t-channel contributions*, *JHEP* **09** (2009) 111, [[arXiv:0907.4076](#)].
- [25] S. Hoche, F. Krauss, M. Schonherr, and F. Siegert, *Automating the POWHEG method in Sherpa*, *JHEP* **04** (2011) 024, [[arXiv:1008.5399](#)].
- [26] E. Re, *Single-top Wt-channel production matched with parton showers using the POWHEG method*, *Eur. Phys. J.* **C71** (2011) 1547, [[arXiv:1009.2450](#)].
- [27] S. Alioli, P. Nason, C. Oleari, and E. Re, *Vector boson plus one jet production in POWHEG*, *JHEP* **01** (2011) 095, [[arXiv:1009.5594](#)].
- [28] S. Alioli, K. Hamilton, P. Nason, C. Oleari, and E. Re, *Jet pair production in POWHEG*, *JHEP* **04** (2011) 081, [[arXiv:1012.3380](#)].
- [29] A. Kardos, C. Papadopoulos, and Z. Trocsanyi, *Top quark pair production in association with a jet with NLO parton showering*, [arXiv:1101.2672](#).

- [30] T. Melia, P. Nason, R. Rontsch, and G. Zanderighi, *W^+W^+ plus dijet production in the POWHEG BOX*, [arXiv:1102.4846](#).
- [31] S. Hoche, F. Krauss, M. Schonherr, and F. Siegert, *NLO matrix elements and truncated showers*, [arXiv:1009.1127](#).
- [32] K. Hamilton, P. Richardson, and J. Tully, *A Positive-Weight Next-to-Leading Order Monte Carlo Simulation for Higgs Boson Production*, *JHEP* **04** (2009) 116, [[arXiv:0903.4345](#)].
- [33] K. Hamilton, *A positive-weight next-to-leading order simulation of weak boson pair production*, *JHEP* **01** (2011) 009, [[arXiv:1009.5391](#)].
- [34] L. D’Errico and P. Richardson, *A Positive-Weight Next-to-Leading-Order Monte Carlo Simulation of Deep Inelastic Scattering and Higgs Boson Production via Vector Boson Fusion in Herwig++*, [arXiv:1106.2983](#).
- [35] L. D’Errico and P. Richardson, *Next-to-Leading-Order Monte Carlo Simulation of Diphoton Production in Hadronic Collisions*, [arXiv:1106.3939](#).
- [36] S. Alioli, P. Nason, C. Oleari, and E. Re, *A general framework for implementing NLO calculations in shower Monte Carlo programs: the POWHEG BOX*, *JHEP* **06** (2010) 043, [[arXiv:1002.2581](#)].
- [37] S. Frixione, E. Laenen, P. Motylinski, and B. R. Webber, *Angular correlations of lepton pairs from vector boson and top quark decays in Monte Carlo simulations*, *JHEP* **04** (2007) 081, [[hep-ph/0702198](#)].
- [38] J. C. Collins, F. Wilczek, and A. Zee, *Low-Energy Manifestations of Heavy Particles: Application to the Neutral Current*, *Phys. Rev.* **D18** (1978) 242.
- [39] F. Maltoni and T. Stelzer, *MadEvent: Automatic event generation with MadGraph*, *JHEP* **02** (2003) 027, [[hep-ph/0208156](#)].
- [40] S. Frixione, Z. Kunszt, and A. Signer, *Three-jet cross sections to next-to-leading order*, *Nucl. Phys.* **B467** (1996) 399–442, [[hep-ph/9512328](#)].
- [41] B. W. Harris and J. F. Owens, *The two cutoff phase space slicing method*, *Phys. Rev.* **D65** (2002) 094032, [[hep-ph/0102128](#)].
- [42] L. Reina, S. Dawson, and D. Wackeroth, *QCD corrections to associated $t\bar{t}H$ production at the Tevatron*, *Phys. Rev.* **D65** (2002) 053017, [[hep-ph/0109066](#)].
- [43] S. Dawson, C. Jackson, L. H. Orr, L. Reina, and D. Wackeroth, *Associated Higgs production with top quarks at the Large Hadron Collider: NLO QCD corrections*, *Phys. Rev.* **D68** (2003) 034022, [[hep-ph/0305087](#)].
- [44] J. A. M. Vermaseren, *New features of FORM*, [math-ph/0010025](#).
- [45] M. Jamin and M. E. Lautenbacher, *TRACER: Version 1.1: A Mathematica package for gamma algebra in arbitrary dimensions*, *Comput. Phys. Commun.* **74** (1993) 265–288.
- [46] M. Cacciari, G. P. Salam, and G. Soyez, *The anti- k_T jet clustering algorithm*, *JHEP* **04** (2008) 063, [[arXiv:0802.1189](#)].
- [47] S. Catani, Y. L. Dokshitzer, M. H. Seymour, and B. R. Webber, *Longitudinally invariant K_T clustering algorithms for hadron hadron collisions*, *Nucl. Phys.* **B406** (1993) 187–224.
- [48] <http://mcfm.fnal.gov>.

- [49] P. M. Nadolsky *et. al.*, *Implications of CTEQ global analysis for collider observables*, *Phys. Rev.* **D78** (2008) 013004, [[arXiv:0802.0007](#)].
- [50] J. M. Butterworth, J. R. Forshaw, and M. H. Seymour, *Multiparton interactions in photoproduction at HERA*, *Z. Phys.* **C72** (1996) 637–646, [[hep-ph/9601371](#)].